Final Report

NASA Grant NGR-33-010-057

for

NUMERICAL SIMULATION OF SMALL PERTURBATION TRANSONIC FLOWS

from

Cornell University
Ithaca, N. Y. 14850

Principal Investigator: A. R. Seebass

Co-Principal Investigator: N. J. Yu

Technical Officer: Leroy L. Presley
NASA Ames Research Center

Period: September 1, 1973-December 31, 1975

Contents:

April 1976

NUMERICAL SIMULATION OF SMALL PERTURBATION TRANSONIC FLOWS

Summary

This report summarizes the results of our systematic study of small perturbation transonic flows during the past year. In our research, both the flow over thin airfoils and the flow over wedges have been investigated. Various numerical schemes have been employed in the study. The prime goal of the research was to determine the efficiency of various numerical procedures by accurately evaluating the wave drag, both by computing the pressure integral around the body and by integrating the momentum loss across the shock. Numerical errors involved in the computations that affect the accuracy of drag evaluations have been analyzed. The factors that affect numerical stability and the rate of convergence of the iterative schemes were also systematically studied. The main results of the study are:

a) The most important factors affecting the accuracy of the numerical solution are the truncation errors, i.e., the errors involved in the difference approximations to the governing equations. For medium size mesh computations, the errors involved in the first-order flux conservative scheme may result in a 20% disagreement in the drag evaluations, although the numerical error in the solution to the difference equations, i.e., $/\Delta\phi/_{max}$, has been reduced to 10^{-5} and the global mass conservation satisfied to 1%.

b) A convergence criterion of $/\Delta\phi/_{max} \leq 10^{-4}$ is adequate for most medium mesh calculations, and further reduction in $/\Delta\phi/_{max}$ does not improve the results significantly.

c) In the calculations of transonic flow over a wedge, the choice of the sonic point operator near the wedge surface is crucial to the numerical behavior. We found that the direct application of Murman's conservative sonic point operator[1] to the wedge calculation usually resulted in an instability. The nonconservative sonic point operator that we used in the past[2] stabilizes the calculations but predicts a smaller supersonic region than the modified conservative sonic point operator that we developed in the course of the present study.

d) The shock strength is affected by the far field boundary data, ϕ, which, in turn, affects the agreement of the drag as evaluated by the pressure integral around the body and by momentum loss across the shock. Several approximate methods of evaluating ϕ in the far field have been discussed in this study, including a compromise approximation that results in good agreement for the drag evaluations.

e) A second-order conservative scheme that we developed can be applied to transonic flow calculations containing an embedded supersonic expansion region with shock waves, such as flow over parabolic-arc airfoils. However. when applied to flow calculations with sharp supersonic compressions, numerical oscillations appear even if some second-order dissipation is added.

f) The shock fitting scheme we proposed [3] is tested in the present study. We conclude that this shock fitting scheme has no great advantage over a flux conservative scheme if the shock transition is of the supersonic-subsonic type although it does capture the Oswatitsch-Zierep singularity more readily. However,

shock fitting does improve the solution in regions of flow containing a supersonic-supersonic shock by eliminating spurious differencing across the shock. Similar conclusions are reported by Hafez and Cheng.[4]

g) For a crude initial guess of ϕ, convergence of iterative procedures can be improved by choosing smaller relaxation factors in the initial stage of calculation[5],[6] and then increasing the relaxation factors in the later stages of calculation. The accelerating iterative scheme advocated by Hafez and Cheng[4] was tested for the calculation of flow over a wedge with a non-uniform mesh distribution. No significant improvement in convergence behavior has been achieved in the present study.

In summary, we are able to calculate small perturbation transonic flows efficiently, including flows with sharp expansions and compressions. To obtain reasonable agreement in wave drag evaluations we still have to rely on the first-order conservative calculations that employ a highly refined mesh. An attractive alternative is to use a higher-order scheme, such as the second-order flux conservative scheme we developed. However, further improvements in the numerical stability of such schemes are necessary in order to make them applicable to a wide class of flows.

1. Introduction

It is inevitable that the next generation of aircraft will take full advantage of the developing technologies in transonic flow. A factor of importance for all aircraft is their cruise efficiency, which is proportional to the product of the aircraft's Mach number and the maximum lift-to-drag ratio that may be achieved at that Mach number.

Increases in near-sonic cruise speeds, increases in aspect ratio, or decreases in structural weight that can be obtained with advanced transonic wing designs will provide for more efficient operation of aircraft provided that these gains are realized without noticeable drag penalties. Aircraft maneuverability, as well as flutter and buffet boundaries, are also of major concern in the transonic regime. How efficiently the aircraft will operate at transonic speeds may depend critically on our ability to calculate transonic flows numerically, and how efficiently these calculations can be embedded in the design process. It will also depend critically on our ability to test and modify such designs on the basis of wind tunnel measurements. Current analytical, experimental and numerical design efforts have been reviewed recently by Boerstoel[7], Cole[8] and Pierpont.[9] Bailey[10], Jameson[11] and Ballhaus[12] have reviewed recent improvements in the computation of steady and nonsteady transonic flows. Such calculations were first performed for airfoils by Murman and Cole[13], and later improved by Murman.[1]

In the last several years the ability to compute such flows has been utilized in design studies, with a computer used to alter the profile shape until given design goals are reached. Work of this nature was initiated in the hodograph plane by Garabedian et al.[14] and by Boerstoel[15], and in the physical plane by Hicks et al.[16] and Barger et al.[17] The ramifications of improved designs for various categories of aircraft are discussed by Pierpont[9], and their particular effect on fuel economy is more fully detailed in Povinelli et al.[18] The design studies of Hicks et al. calculate the lift and drag of a sequence of airfoils, each perturbed slightly from the previous one,

seeking changes that improve their performance. An important goal of such calculations is to reduce the wave drag of the airfoils to a minimum over a range of Mach numbers with the lift, maximum adverse pressure gradient, surface area, etc., constrained. Consequently, it is important that such studies use a numerical code that predicts the wave drag accurately. The usual relaxation procedures used are probably adequate for this purpose if there are no rapid expansions in the flow, if the airfoil is not too highly curved where the shock wave meets it, and if a highly refined mesh is used (see, e.g., Murman's calculation for the parabolic-arc[19]). However, the airfoils that look most attractive usually have quite rapid expansions in the flow and the number of airfoils that are examined in an optimization procedure may be large, precluding calculations with a highly refined mesh. If the calculations involve modest errors in the evaluation of the wave drag, an improper optimum may be selected. Current computers are fast enough that calculations with highly refined mesh spacings can be used to resolve this dilemma in two dimensions, but the optimization of swept wings and additional design studies on two dimensional airfoils may benefit from numerical procedures that insure that the wave drag is computed accurately and reasonably efficiently.

This report addresses the basic difficulty encountered in the accurate evaluation of the wave drag, and suggests appropriate remedies for this difficulty as well as for other sources of error in these computations. We illustrate this basic point by considering the following simple mixed-flow problem:

$$(K + \phi_x)\,\phi_{xx} - \phi_{yy} = 0, \qquad \epsilon D,$$

$\phi_y(x,0) = f(x)$ on $[0,1]$, $\quad \phi_y(x,0) = 0$ elsewhere, (P)

and $\phi \to 0$, as $x^2 + y^2 \to \infty$,

where D is the upper-half plane.

The problem (P) is an appropriately scaled representation of transonic flow past a nonlifting body. Here we deal with a perturbation potential ϕ, and consequently restrict f(x) such that $f(x) \leq 1$. The parameter K is the usual transonic similarity parameter $(M_\infty^2 - 1)/(\delta(\gamma + 1))^{2/3}$.

The partial differential equation of the problem (P) is nonlinear and admits weak, i.e., discontinuous solutions. These discontinuities are the irrotational small perturbation approximation to the shock waves that arise in the real flow. Because the perturbations are small and the flow Mach number close to 1, the vorticity introduced by these shock waves is sufficiently small that it may be justifiably neglected. There is, however, the question of the proper embedding of these discontinuous solutions in the physical framework that gives rise to the approximation (see, e.g., Dafermos[20]). This is accomplished by noting that (P) is the analog of the conservation of mass, and that the solution to the difference equation that represents (P) should insure that mass is conserved, not only where the flow is continuous, but also across any discontinuities that arise.[10, 19] Hence the equation is more appropriately written in the form

$$\nabla \cdot \underline{M} = 0, \text{ where } \quad \underline{M} = \frac{1}{2}(K + \phi_x)^2 \, \underline{i} - \phi_y \, \underline{j}. \tag{1}$$

The auxiliary condition,

$$\nabla \cdot \underline{q} = 0, \quad \text{where} \quad \underline{q} = \phi_y \, \underline{i} - \phi_x \, \underline{j}, \tag{2}$$

is needed to specify the shock jump conditions.

We seek solutions to (1) by noting that if (1) and (2) are judged to be the basic conservation laws of the problem from which (P) derives, then

$$(dy/dx)_{\text{discontinuity}} = -[M_y]/[M_x] = -[\phi_x]/[\phi_y],$$

where [ ] indicates the jump across the discontinuity in the bracketed entity. From (1) and (2), we find

$$(K + \tilde{\phi}_x)\ [\phi_x]^2 = [\phi_y]^2, \tag{3}$$

where $\tilde{(\ )}$ means the mean of the value of ( ) evaluated on each side of the discontinuity.

This representation of shock waves insures the conservation of mass but does not allow any vorticity to be generated and hence requires a loss in the axial momentum flux across the discontinuity. This corresponds to the wave drag that results from the shock wave. This momentum loss must correspond to a force on the body and, consequently, to the drag given by the integral of the pressure over the body. The mathematical form of this statement derives directly from the perturbed axial momentum flux given by

$$\nabla \cdot \underline{N} = 0, \text{ where } \underline{N} = \left(\tfrac{1}{2} K\phi_x^2 + \tfrac{1}{3} \phi_x^3 + \tfrac{1}{2} \phi_y^2\right) \underline{i} - \phi_x \phi_y \underline{j}. \tag{4}$$

Using the divergence theorem, one can convert the surface integral of $\nabla \cdot \underline{N}$ to a line integral with the contour of integration shown in figure 1 containing the body, the discontinuity and the far-field boundary. Applying the relation (3) across the discontinuity cd, the pressure integral around the body, ab, is related to the jump in ϕ_x along cd by

$$\int_{ab} \phi_x \phi_y \, dx = -1/12 \int_{cd} [\phi_x]^3 \, dy. \tag{5}$$

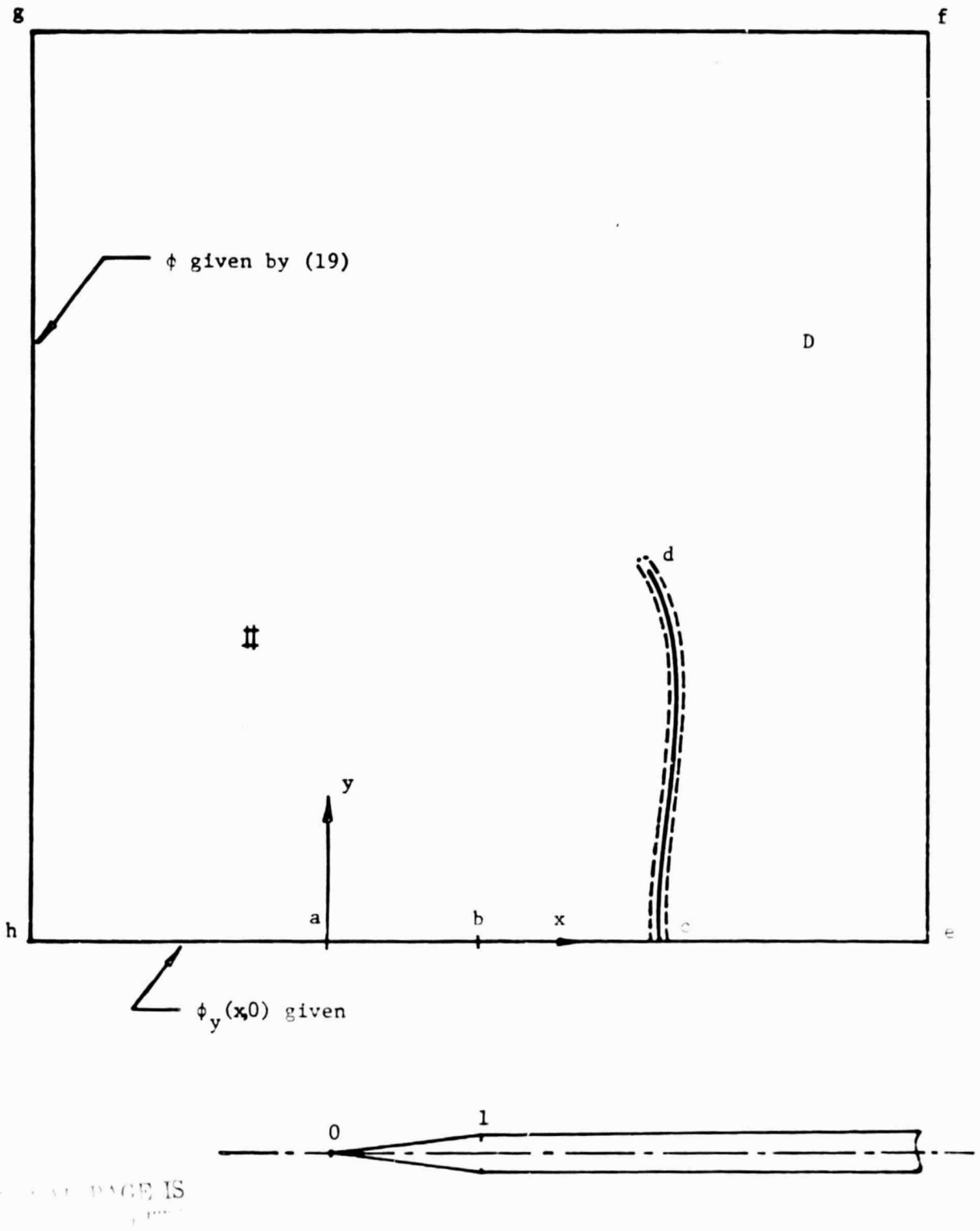

Figure 1. Region of computation for flow over a wedge.

Equation (5) can also be derived directly from the surface integral of the x-momentum equation around region D, i.e.,

$$\int\int_D \nabla \cdot \{(p + \rho u^2)\ \underline{i} + \rho uv\ \underline{j}\}\ dxdy = 0.$$

Introducing the small disturbance approximation to the above equation and keeping terms of $O(\delta^{4/3})$, one obtains the same relation (5) between the pressure integral and momentum loss along the shock.[10]

Various numerical schemes that solve (P) with the proper jump relations satisfied across the discontinuity are discussed. The numerical difficulties encountered in the study and the methods used to overcome such difficulties are detailed in the following sections.

2. Numerical Procedures

A. Difference approximations

The well-known type-dependent difference approximations developed by Murman and Cole[13] and modified by Murman[1] are adopted in the present study. The difference approximations are constructed such that in the supersonic region the domain of dependence is properly accounted for and the difference equation for (P) satisfies conservation of mass. After briefly reviewing this first-order scheme we discuss other schemes that we have used.

i. First-order scheme:

Detailed discussion of the fully conservative first-order scheme for transonic flow calculations can be found in Murman[1] and also in Jameson.[11] An essential point is that at every computational point the coefficient $K = \phi_x$ is computed first to determine the type of equation for (P). If the computational

point is a subsonic point, central difference approximations are used for all derivatives in (P); if it is a supersonic point, backward difference approximations are used for the streamwise derivative, i.e., the x-derivative in (P). At subsonic-supersonic and supersonic-subsonic transitions, a sonic point operator and the shock point operator are used, respectively, to insure the exact cancellation of all internal mass fluxes generated by the sudden change in the difference approximations. For the problem (P), the sonic point operator is equivalent to the central difference approximation to $\phi_{yy} = 0$, and the shock point operator is represented by the sum of the subsonic difference approximations and the supersonic difference approximations to the x-derivatives, i.e..

$$\{(K + \phi_x)\ \phi_{xx}\}_{\text{subsonic}} + \{(K + \phi_x)\ \phi_{xx}\}_{\text{supersonic}} - \phi_{yy} = 0. \tag{6}$$

Through the use of the above difference approximations, the total mass flux in a given computational region is conserved. Notice that the difference approximation (6) is inconsistent with equation (P). However, across a discontinuity, the differential equation (P) is of little consequence, where the basic conservation law is imperative. In the region of smooth subsonic-supersonic transition, the sonic point operator is consistent with the governing differential equation (P). Applications of the above fully conservative scheme to the calculations of flow over an airfoil are quite successful

and efficient. The shock wave embedded in the flow field is represented by a sharp transition covering about three to four grid points, and the shock strength is correctly represented. Typical results for flow over a parabolic-arc airfoil are represented in figure 2. If this is applied without modification to the calculations of transonic flow over a wedge with a sharp shoulder, an instability occurs that originates in the sonic region near the wedge surface. Because the difference approximation at supersonic points is unconditionally stable and is dissipative, the source of instability must come from the sonic point operator. We used Jameson's time-like analysis for the iterative procedure, applied to the sonic point operator, to show that it is non-dissipative and there is no damping term in the time-like equation. We believe this to be the cause of instability. Let ϕ^* represent the intermediate value ϕ in the iterative process, and ϕ^{n+1} the value of ϕ at the "n+1" iteration and ϕ^n that of the nth iteration, then,

$$\phi^*_{i,j+1} - 2\phi^*_{i,j} + \phi^*_{i,j-1} = 0, \tag{7a}$$

$$\phi^{n+1}_{i,j} = \phi^n_{i,j} + w\,(\phi^*_{i,j} - \phi^n_{i,j}). \tag{7b}$$

Here column (x-line) relaxation is used, with w denoting the relaxation factor. The subscripts "i" and "j" represent the conventional x- and y-grid locations, respectively. If we introduce the following "time-derivative" for the iterative process, i.e.,

$$\phi_t^{n+1} = (\phi^{n+1} - \phi^n)/\Delta t, \tag{8}$$

then we find

$$\phi^* = (1-w)\Delta t/w\ \phi_t^{n+1} + \phi^{n+1}. \tag{9}$$

Substituting (8) and (9) into the sonic point equation, one obtains the time-like equation for the sonic point

$$\phi_{yy}^{n+1} + (1-w)\ \Delta t/w\ \phi_{tyy}^{n+1} = 0. \tag{10}$$

Equation (10) has no damping in t as $\Delta t \to 0$ and hence there is difficulty with rapid expansions. Thus an initial error that appears at the sonic point may not decay as the iteration proceeds. The numerical oscillation of $/\Delta\phi/$ at the sonic point for wedge calculations is a typical example of such instability. This instability may not appear if the flow expands smoothly from subsonic to supersonic, such as in the calculations of flow over a parabolic-arc airfoil. There is a simple amendment to eliminate such instability, but this is at the expense of losing the conservative property at the sonic transition. A combination of the backward difference approximation to $K + \phi_x$ and the central difference approximation to ϕ_{xx} provide sufficient damping and thus control the instability. Let $q = (K + \phi_x)_b \leq 0$ at the sonic point; the difference equation is given by

$$q\ \phi_{xx_c} - \phi_{yy_c} = 0, \tag{11}$$

where subscript "b" refers to the backward difference

approximation and "c" to the central difference approximation. Again, if (8) and (9) are introduced to (11), one has

$$q\,\phi_{xx}^{n+1} - \phi_{yy}^{n+1} - \left(\frac{q\Delta t}{\Delta x^2}\right)\left(\frac{2-w}{w}\right)\phi_t^{n+1} = 0. \tag{12}$$

Equation (12) is diffusive in t if $w \leq 2$; therefore, iterative procedures with sonic point operator (11) will be stable. Numerical tests for flow over a wedge and flows over airfoils confirm the above statement.

An alternative way of stabilizing the calculations is to treat the flow near the sharp wedge shoulder more accurately. For a subsonic freestream condition, the sonic point on the wedge surface must appear at the shoulder, i.e., point "b" in figure 1. This gives

$$K + \phi_{x_b} = 0. \tag{13}$$

Equation (13) can be used to determine the value of ϕ at the point right behind the shoulder, say, point "i+1,1",

$$\phi_{i+1,1} = \phi_{i,1} - K\Delta x. \tag{14}$$

At other sonic points Murman's fully conservative sonic point operator is used. With the above implementation, the iteration along the column just downstream of the shoulder becomes a fixed boundary value iteration in ϕ, instead of an iteration with a given ϕ at one end and ϕ_y at the other. The simple modification (14) at the wedge shoulder stabilizes the relaxation procedures and shows a convergence behavior similar

to the non-conservative sonic point operator (11). For the wedge calculations, the numerical results using (11) and (14) are quite different; this difference will be discussed later.

ii. Second-order scheme

The first-order scheme usually provides results with poor resolution if only a moderate number of computational points are employed. To obtain better resolution for the calculations with a given total number of computational points, the natural alternative is to use a higher-order scheme. The simplest higher-order conservative scheme is the second-order scheme. Following procedures analogous to those for the first-order flux conservative scheme, one can construct a second-order flux-conservative scheme for the supersonic region, viz.,

$$\phi_x = (2\phi_{i,j} - \phi_{i-1,j} - 2\phi_{i-2,j} + \phi_{i-3,j})/2\Delta x + \frac{5}{6}\Delta x^2 \phi_{xxx},$$

$$\phi_{xx} = (2\phi_{i,j} - 5\phi_{i-1,j} + 4\phi_{i-2,j} - \phi_{i-3,j})/\Delta x^2 + \frac{11}{12}\Delta x^2 \phi_{xxxx}. \quad (15a,b)$$

The corresponding sonic point operator and shock point operator for the x-derivatives are:

Sonic point operator:

$$\phi_x = (3\phi_{i,j} - 4\phi_{i-1,j} + \phi_{i-2,j})/2\Delta x + \frac{1}{3}\Delta x^2 \phi_{xxx},$$

$$\phi_{xx} = (\phi_{i,j} - 2\phi_{i-1,j} + \phi_{i-2,j})/\Delta x^2 + \Delta x\, \phi_{xxx}; \quad (16a,b)$$

Shock point operator:

$$\phi_x = (\phi_{i+1,j} - \phi_{i,j} + 2\phi_{i-1,j} - 3\phi_{i-2,j} + \phi_{i-3,j})/2\Delta x + \frac{1}{3}\Delta x^2 \phi_{xxx},$$

$$\phi_{xx} = (\phi_{i+1,j} - \phi_{i,j} - 2\phi_{i-1,j} + 3\phi_{i-2,j} - \phi_{i-3,j})/\Delta x^2 - \Delta x \phi_{xxx}. \qquad (17a,b)$$

To insure the correct transition, the sign of the type dependent coefficient, $K + \phi_x$, is calculated by the difference approximations used in the first-order scheme. The detailed construction of this second-order scheme is given in Appendix A. Notice that the supersonic expansion region, dissipative and dispersive truncation errors are of the same order and that in supersonic compressions the truncation errors are non-dissipative. The dominant error is dispersive and serious numerical difficulties are encountered. Procedures that avoid these difficulties are still under investigation. One of the methods which has been proved effective in the calculations of flow with an embedded supersonic expansion region terminated by a shock, is to add a conservative dissipation term to the governing equation, i.e.,

$$(K+\phi_x)\phi_{xx} - \phi_{yy} = C\Delta x^2 (k\phi_{xx})_x, \text{ with } C \geq 0, \qquad (18)$$

where k is a function which has the value of 0 or 1 to insure that the added term is also flux conservative. The difference approximation of $(k\phi_{xx})_x$ in each region is given below:

Supersonic region: $k_i = k_{i-1} = 1$

$$(k\phi_{xx})_x = (1/\Delta x)(k_i\ \phi_{xx_i} - k_{i-1}\ \phi_{xx_{i-1}})$$

$$= (1/\Delta x^3)(\phi_i - 3\phi_{i-1} + 3\phi_{i-2} - \phi_{i-3})$$

Sonic region: $k_{i-1} = 0,\ k_i = 1$

$$(k\phi_{xx})_x = (1/\Delta x^3)(\phi_i - 2\phi_{i-1} + \phi_{i-2})$$

Shock region: $k_i = 0,\ k_{i-1} = 1$

$$(k\phi_{xx})_x = (1/\Delta x^3)(\phi_{i-1} - 2\phi_{i-2} + \phi_{i-3}).$$

One can change the coefficient C to control the magnitude of the dissipation. Normally, one should choose C to be O(1) to insure that the scheme is still second-order accurate. This scheme was tested for flow over a parabolic-arc airfoil at different Mach numbers using the results of the first-order calculations for the initial guess. We found the above scheme to be stable. The pressure distribution along the surface is shown in figure 2a. When we applied the same procedure to the flow over a wedge the value of C had to be increased by a factor of 10 to damp the dispersive errors. The error, $/\Delta\phi/_{max}$, remains bounded and decreases slowly, but the pressure distribution just behind the shoulder still exhibits oscillations, which in turn affects the shock strength during the iterative process. We suspect that a second, weak shock in the shoulder region may

cause oscillation. However, the existence (or nonexistence) of a second shock can not be established with current numerical calculations.

iii. Shock fitting scheme:

We, as well as others (notably Hafez and Cheng[4], Moretti[21]), have advocated treating the shock wave as a discontinuity in the computations. As discussed in reference 3, shock fitting not only provides a more reliable solution in the shock region by eliminating the large truncation errors due to improper differencing, but also saves a considerable amount of computing time by avoiding the unnecessary mesh refinement in the shock region. In the study of transonic flow with an embedded shock, we have introduced a shock-fitting scheme in conjunction with relaxation procedures. Detailed implementation of shock fitting to the relaxation procedures has been given in reference 2 and is summarized in Appendix B. A convergent solution can easily be obtained, and the results show the expected singularity when the shock intersects the curved surface, even with a rather crude mesh. We have compared the results of shock fitting with flux conservative calculations and found that both schemes provide solutions with well-defined supersonic-subsonic shocks; shock fitting provides a true discontinuity shock, while the flux conservative schemes give shock transitions covering 3-4 grid points. For most of the numerical studies, the shock transition that covers 3 or 4 grid points is considered rather successful.

Thus, we believe that in transonic flow problems containing only supersonic-subsonic shocks the flux conservative scheme is adequate and is easier to implement than shock-fitting scheme. For flow calculations containing a supersonic-supersonic shock, where a flux conservative scheme provides poor resolution for the shock, shock fitting is bound to be of practical importance.

A caveat is in order here. We have found that if shock fitting is introduced with the shock in the wrong position, located say, by a nonconservative calculation, the values of ϕ may change so that the jump conditions are satisfied but the shock may not move to the location predicted by a conservative calculation (without shock fitting). This "nonunique" behavior is believed to be due to the fact that changes in ϕ behind the shock, required by shock fitting, are accommodated erroneously in the nonlinear contribution to far-field boundary data rather than effecting data near the sonic line and hence the shock position. The use of shock fitting in conjunction with a fast Poisson solver needs to be implemented to see if this resolves the difficulty.

B. Evaluation of far field

All the calculations shown in this report are carried out in a finite computational region. That is, we avoided mapping an infinite domain to a finite one. Thus, an approximate formula to evaluate ϕ on the boundaries is necessary. We used Klunker's[22] representation,

$$\phi = \frac{1}{2\pi\sqrt{-K}}\left\{\int_0^1 f(\xi)\log\left[(x-\xi)^2 - Ky^2\right]d\xi\right.$$

$$\left. + \frac{1}{2}\int\int_{-\infty}^{\infty} \phi_x^{\,2}\,\frac{x-\xi}{(x-\xi)^2 - K(y-\eta)^2}\,d\xi d\eta\right\}, \tag{19}$$

where the first term represents the source contribution due to the body, and the second term the nonlinear contribution throughout the flow field. Direct evaluation of the nonlinear contribution requires tedious double integration at every boundary point and proves to be extremely time-consuming. An alternative is to pull out the kernel $(x-\xi)/\{(x-\xi)^2-K(y-\eta)^2\}$ and evaluate it at a mean position such that the double integral is calculated just once and used for all boundary points; i.e.,

$$\int\int_{-\infty}^{\infty} \phi_x^{\,2}\,\frac{x-\xi}{(x-\xi)^2-K(y-\eta)^2}\,d\xi d\eta = \frac{x-x_{av}}{(x-x_{av})^2-K(y-y_{av})^2}\cdot$$

$$\int\int_{-\infty}^{\infty} \phi_x^{\,2}\,d\xi d\eta. \tag{20}$$

A good approximation for (x_{av}, y_{av}) for a symmetric problem is $(\frac{1}{2}, 0)$, i.e., at the center point of the chord. One can also obtain a higher order approximation by a series expansion of the kernel with respect to $\xi - \sqrt{K}\eta/x - \sqrt{K}y$ and $\xi + \sqrt{K}\eta/x + \sqrt{K}y$, i.e.,

$$(x-\xi)/\{(x-\xi)^2 - K(y-\eta)^2\} = 1/(x^2-Ky^2)\left\{x + \frac{x^2+Ky^2}{x^2-Ky^2}\,\xi\right.$$

$$\left. - \frac{2x}{x^2-Ky^2}\,\xi^2 - \frac{2Kxy}{x^2-Ky^2}\,\eta - \frac{2Ky}{x^2-Ky^2}\,\xi\eta + \ldots\right\} \tag{21}$$

In the above representation, one has to evaluate

$$\int\int \xi\phi_x^2 d\xi d\eta, \quad \int\int \xi^2\phi_x^2 d\xi d\eta, \quad \int\int \eta\phi_x^2 d\xi d\eta \text{ and}$$

$$\int\int \xi\eta\phi_x^2 d\xi d\eta \text{ in addition to } \int\int \phi_x^2 d\xi d\eta.$$

These integrations can be obtained with little extra computational effort over that required to evaluate $\int\int \phi_x^2 d\xi d\eta$. We have used the above expansion for the calculations of far field ϕ, and found its effect on the results is negligible if the size of the computational region is large enough, say, 5 by 5 chord lengths. But it is important that x_{av} and y_{av} be chosen rationally. This fact is illustrated in section 3.

C. Convergence criteria

The iterative procedures terminate when the numerical solution to the difference equations reaches a prescribed accuracy. There are many ways of defining numerical accuracy. The most common one is to set the maximum change in ϕ throughout the computational field at each successive iteration to be less than a small quantity, ε, i.e., $/\Delta\phi/_{max} \leq \varepsilon$. For most of the calculations, an ε of 10^{-4} or 10^{-5} is enough. Further reduction in ε gives a more accurate solution to the difference equations but not necessarily to the differential equation unless finer meshes are used.

Another way of defining convergence is to require that the residual of the difference equation at each computational point be less than a given small number. Normally, for given accuracy

in $/\Delta\phi/_{max}$, the residual of the difference equation is at least one order of magnitude larger than $/\Delta\phi/_{max}$. Thus, using the maximum residual in the field as a convergence criterion is more restrictive than computing ϕ to the same accuracy. In this report, we use $/\Delta\phi/_{max} \leq 10^{-5}$ unless specifically mentioned.

D. Relaxation factors and acceleration schemes

The convergence behavior of the relaxation procedures depends on the choice of relaxation factors. In some cases, an improper guess of relaxation factors causes the scheme to diverge. Because the problem (P) is nonlinear, there is no simple way of finding optimal relaxation factors. The choice of the best relaxation factors usually relies on numerical experiments. As a general rule it has been found that it is better to choose smaller relaxation factors in the initial stage of the calculations, including both the subsonic over-relaxation factor and the supersonic under-relaxation factor. In the later stage of calculations, one should increase the relaxation factors to as large a value as possible (within the limit of stability criteria) to enhance the convergence. Normally, the upper limits of the relaxation factors for medium mesh calculations are 1.95 for the subsonic region and 0.90 for the supersonic region.

For nonuniform mesh calculations, little is known about the choice of relaxation factors. We have experienced a slow rate of convergence for a range of relaxation factors. In most cases, for a given relaxation factor, the rate of convergence for non-uniform x- and y-mesh distribution is slower than that of uniform

mesh distribution. Further investigations are necessary in order to improve the efficiency of the relaxation procedures.

The accelerated iterative scheme proposed by Hafez and Cheng has also been tested on the calculations of flow over a wedge using non-uniform mesh distribution. We were not able to achieve the fast rates of convergence reported by Caughey and Jameson.[23] The extrapolated value ϕ for each accelerated step usually increases the errors in ϕ rapidly, and the relaxation step following the accelerated step decreases the errors to the previous level. Such behavior repeats in the iterative process, which in turn provides little gain over a pure relaxation scheme. We believe such behavior is caused by the poor estimation of the dominant eigenvalue for the iterative matrix using a non-uniform mesh distribution. The difficulty of finding an accurate estimate of the dominant eigenvalue may restrict general application of accelerated iterative schemes.

Recently, we have tried the acceleration scheme proposed by Jameson[11], i.e., a Poisson solver step followed by a relaxation step. The Poisson solver computes the subsonic region efficiently, where the relaxation step determines the numerical solution in the supersonic region. This improves the rate of convergence at least of one order of magnitude. We found the scheme works fairly well in the physical plane for the calculations of the small perturbation equation. The Poisson solver we used was obtained from NCAR and solves Poisson's equation for a uniform grid. In our test calculations, each Poisson solver step is followed by a few relaxation steps, say 5 to 10 steps. Detailed discussion on such

a scheme will be submitted in a report on a subsequent grant. Typical convergence rates for the combined scheme are shown in figure 7. The solution converges to $/\Delta\phi/_{max} \leq 10^{-6}$ within 100 relaxation steps and 20 Poisson solver steps.

3. Results and Discussions

Most of the present numerical results were obtained using uniform grid calculations. In the case of flow over a sharp wedge, highly non-uniform mesh distributions along both x- and y-direction have also been used. The smallest meshes used in the wedge calculations were $\Delta x = 0.01$ in the nose and shoulder regions, and $\Delta y = 0.01$ near the wedge surface. The mesh increases exponentially away from the nose, the shoulder, and the wedge surface. The region of computation for non-uniform mesh distribution is, in general, much larger than that of uniform mesh distribution. The typical size of the computational region for a uniform mesh distribtuion is 6 by 6 chord lengths, while for a non-uniform mesh distribution it is 25 by 15 chord lengths. In the airfoil calculations, it has been reduced to 3 by 3 chord lengths when the embedded supersonic region is relatively small.

Figure 2a depicts the pressure distributions $Cp = -2(K + \phi_x)$ along the parabolic-arc at $M_\infty = 0.909$. The solid line is the result of a first-order scheme with $\Delta x = \Delta y = 0.05$. The "·" points are the results of a second-order scheme using the same mesh size. Because of the smooth supersonic expansion, there is no significant difference in pressure distribution away from the shock. Figure 2b shows the pressure distributions for the same airfoil at $M_\infty = 0.9$, using both fine mesh (solid line) and coarse mesh first-order calculations.

Again, the results are quite similar, except the fine mesh calculations give a sharper shock. The wave drag, calculated from the results of each scheme for $M_\infty = 0.909$, are listed in the following table, where subscript "PI" refers to the drag evaluated by pressure integral around the body, and "SK" by the momentum loss across the shock.

Table 1. Comparison of wave drag for parabolic-arc at $M_\infty = 0.909$

Scheme	$C_{D(PI)}$	$C_{D(SK)}$
1st order	0.02875	0.02888
2nd order	0.02886	0.02918
Murman[19] refined mesh	0.0315	0.0320

The agreement between $C_{D(PI)}$ and $C_{D(SK)}$ within each scheme is extremely good for this particular case, i.e., approximately 1%. However, using the same mesh distribution, we computed the drag for $M_\infty = 0.9$, and found $C_{D(PI)}$ and $C_{D(SK)}$ differ by 12.5%, (0.0214 vs. 0.0245). The disagreement is reduced to 5% (0.0229 vs. 0.0240) by halving the x-mesh spacing. Thus, we conclude that the drag evaluation is rather sensitive to the numerical approximation to the solution of the differential equation, i.e., to the truncation errors of the difference approximations. This will be discussed further in another report.

Figure 3 illustrates the supersonic region for flow over a wedge at $K = -0.5$. Curve 1 shows the sonic line and shock obtained by using the non-conservative sonic point operator and curve 2 that for the fully

conservative sonic point operator. Because of the sharp expansion around the shoulder, the results are extremely sensitive to the change of difference approximations to the differential equation in that region. The non-conservative sonic point operator pushes the sonic line approximately 2 meshes ahead of the shoulder, whereas the modified conservative sonic point operator (equation 13) predicts the correct sonic condition at the shoulder. Inaccuracy in locating the sonic line may cause an incorrect expansion near the shoulder, which, in turn, results in an incorrect shock position. The pressure distributions along the wedge are shown in figure 4. Because conservative shock point operators were used for both calculations, the jump across the shock satisfies the normal shock relation even though the shock positions are quite different. The drag values for each case are listed in Table 2.

Table 2. Wave drags for flow over wedge at K = -0.5.

Scheme	$C_{D(PI)}$	$C_{D(SK)}$
Non-conservative sonic point operator	0.6535	0.5196
Conservative scheme	0.7627	0.6577
Conservative scheme with modified B.C.	0.7561	0.7577

The flux conservative scheme gives slightly better agreement between $C_{D(PI)}$ and $C_{D(SK)}$ than do non-conservative sonic point calculations. The cause of poor agreement between $C_{D(PI)}$ and $C_{D(SK)}$, as mentioned before, is due to truncation errors. In wedge calculations, we found

that $C_{D(PI)}$ is insensitive to the iteration process, i.e., $C_{D(PI)}$ approaches its final value much faster than $C_{D(SK)}$. The reason is that flow on the wedge surface that contributes to drag evaluation is subsonic. The inaccuracy in the supersonic region has little effect on its pressure distribution. In contrast, $C_{D(SK)}$ is affected by the numerical accuracy in the supersonic region. Thus, for the wedge, $C_{D(PI)}$ is more reliable than $C_{D(SK)}$.

In the calculation of flow over a wedge, the truncation errors around the shoulder cannot be reduced unless a much refined mesh is used. The shock is improperly calculated because of the inaccurate expansion near the shoulder. One way of obtaining agreement between the two evaluations of wave drag is to modify the far-field boundary data. The boundary data for ϕ can be redistributed by evaluating the kernel in (19) at different positions. Because $C_{D(PI)}$ is insensitive to iteration, one can expect that a slight modification of (19) will not change the pressure distribution around the wedge significantly. However, $C_{D(SK)}$ is sensitive to the iteration. Therefore, a redistribution of boundary data ϕ can result in a significant change in shock strength. We have shifted the kernel successively to (-0.25, 0) and found a good agreement in $C_{D(PI)}$ and $C_{D(SK)}$, as shown in Table 2. Interestingly enough, the global conservation of mass has not been affected by the modification of boundary data ϕ, i.e., the unbalanced flux is still within 1%. This simply illustrates the sensitivity of the results to the far-field boundary data. The choice (-0.25, 0) is not consistent with the evaluation of the full integral (19). We conjecture that the large truncation errors in (4) are compensated for by this erroneous evaluation ϕ on the boundary.

To confirm that the disagreement in $C_{D(PI)}$ and $C_{D(SK)}$ is due to large truncation errors near the sharp shoulder, we have carried out the same calculations for the case of a smooth shoulder, i.e.,

$$\phi_y = C, \quad \text{for} \quad 0 \le x \le 0.5,$$

$$\phi_y = C \cos\{\pi(x-0.5)\}, \quad \text{for} \quad 0.5 < x \le 1, \tag{22}$$

with $C = 2\pi/(\pi + 2)$ such that the thickness of the wedge is equal to 1. The pressure distribution for a smooth wedge is shown in figure 5. The discrepancy between $C_{D(PI)}$ and $C_{D(SK)}$ is reduced to 6% (i.e., 0.5185 vs. 0.4845). One can also shift the kernel in (19) to (0.25, 0) instead of (-0.25, 0), and obtain an excellent agreement in $C_{D(PI)}$ and $C_{D(SK)}$ (i.e., 0.5142 vs. 0.5106).

The pressure distribution along a sharp wedge using highly non-uniform mesh calculations is shown in figure 6. Except for a sharper compression downstream of the shoulder, the general feature of the pressure distribution is quite similar to that of uniform mesh calculations.

The results of a shock-fitting calculation have been included in the previous report and also presented in reference 2, and will not be repeated here. Shock fitting does provide better resolution in the shock region. However, the discrepancy in $C_{D(PI)}$ and $C_{D(SK)}$ in the wedge calculations, which is due mainly to poor resolution near the expansion region (the shoulder) cannot be improved by shock fitting.

In figure 7 we showed the convergence behavior for both sharp wedge and smooth wedge calculations. For a pure relaxation scheme the smoother flow has better convergence. Typically, it requires 500 iterations or more to bring the error $/\Delta\phi/_{max}$ down to 10^{-5}.

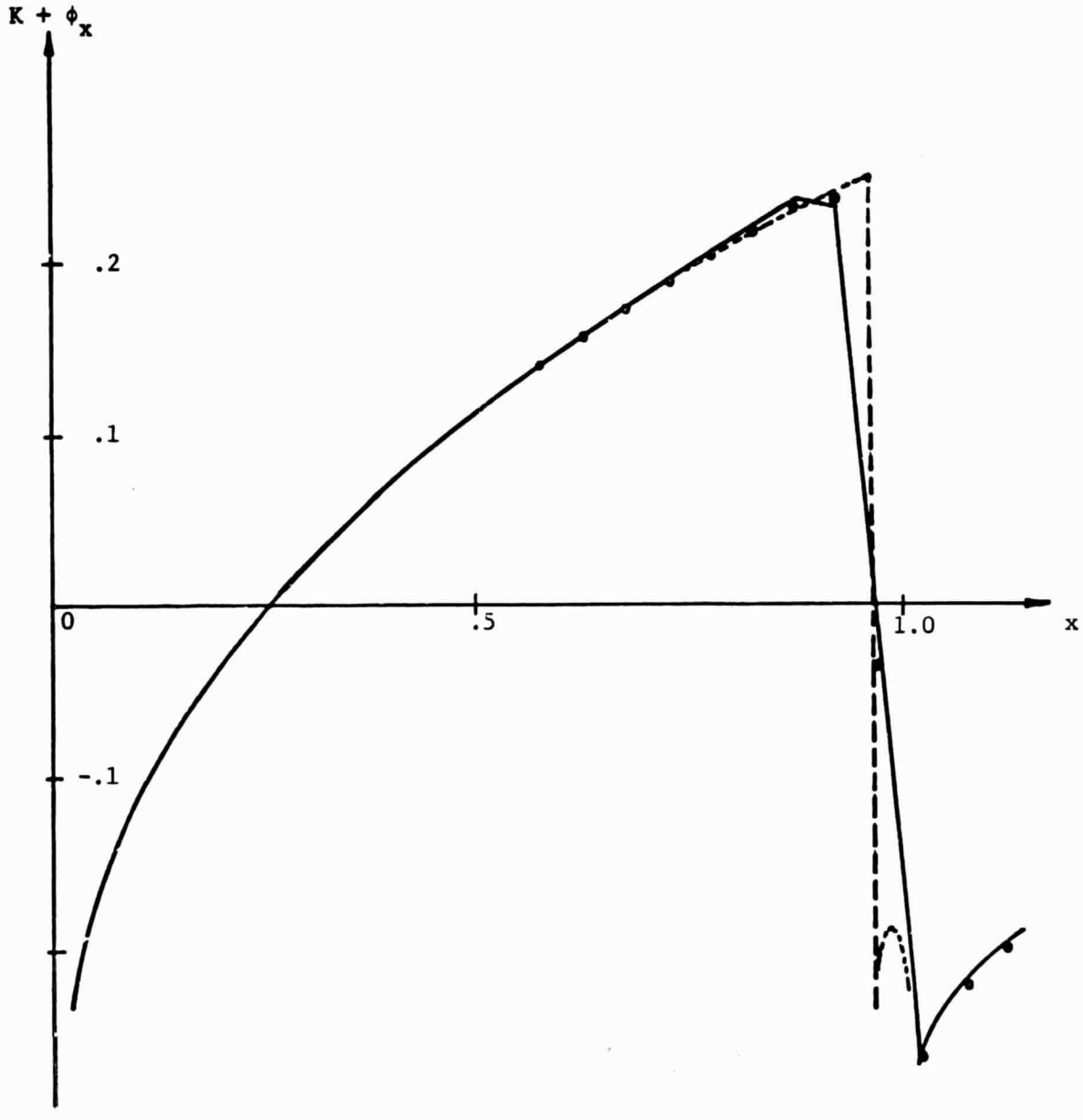

Figure 2a. Pressure distribution along a parabolic-arc airfoil at $M_\infty = 0.909$. _____: first-order scheme. ".": second-order scheme. ---: with shock fitting. See Table 1.

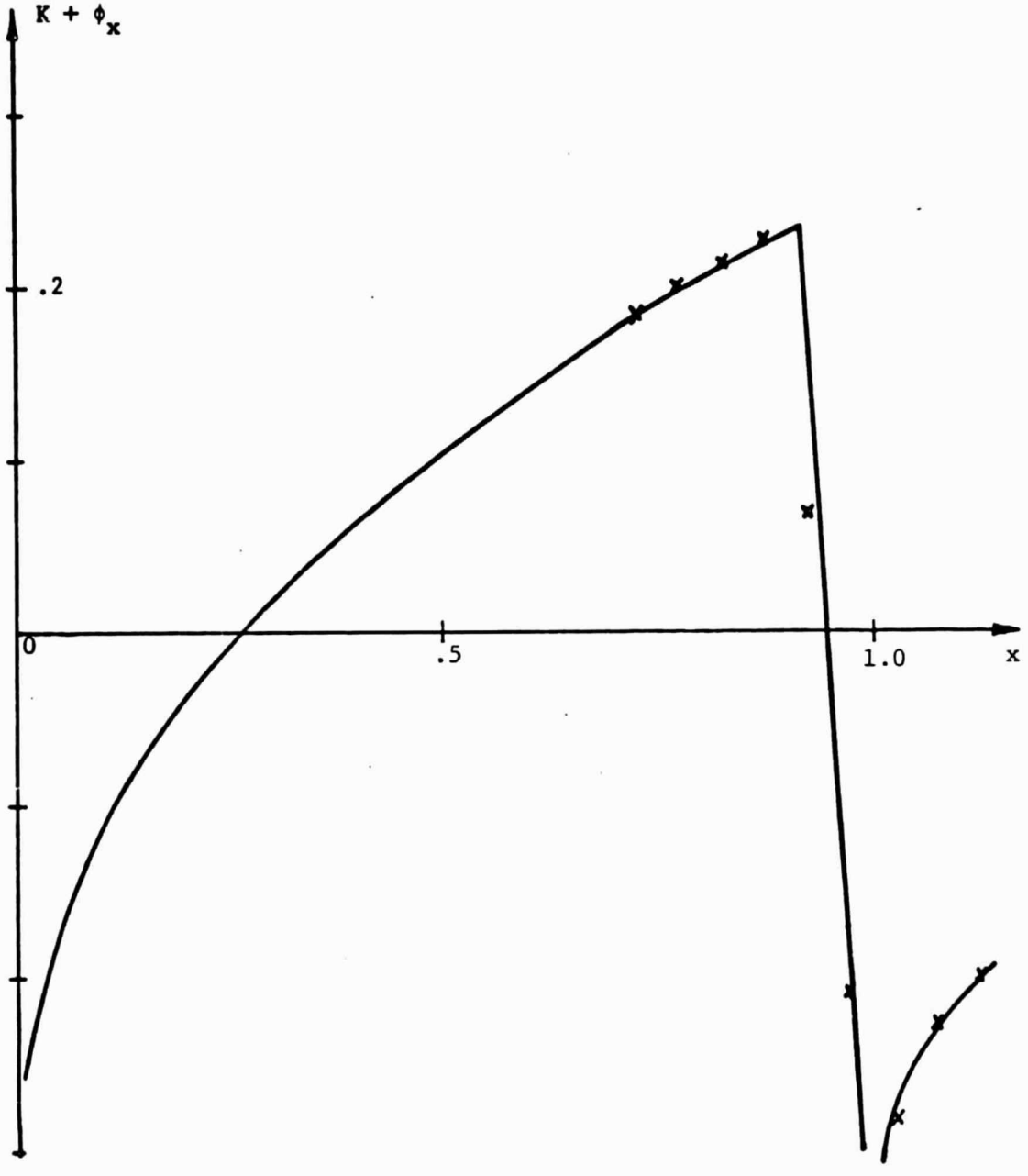

Figure 2b. Continued. M_∞ = 0.900. First-order scheme, ———: fine mesh; "x": crude mesh. See text following Table 1.

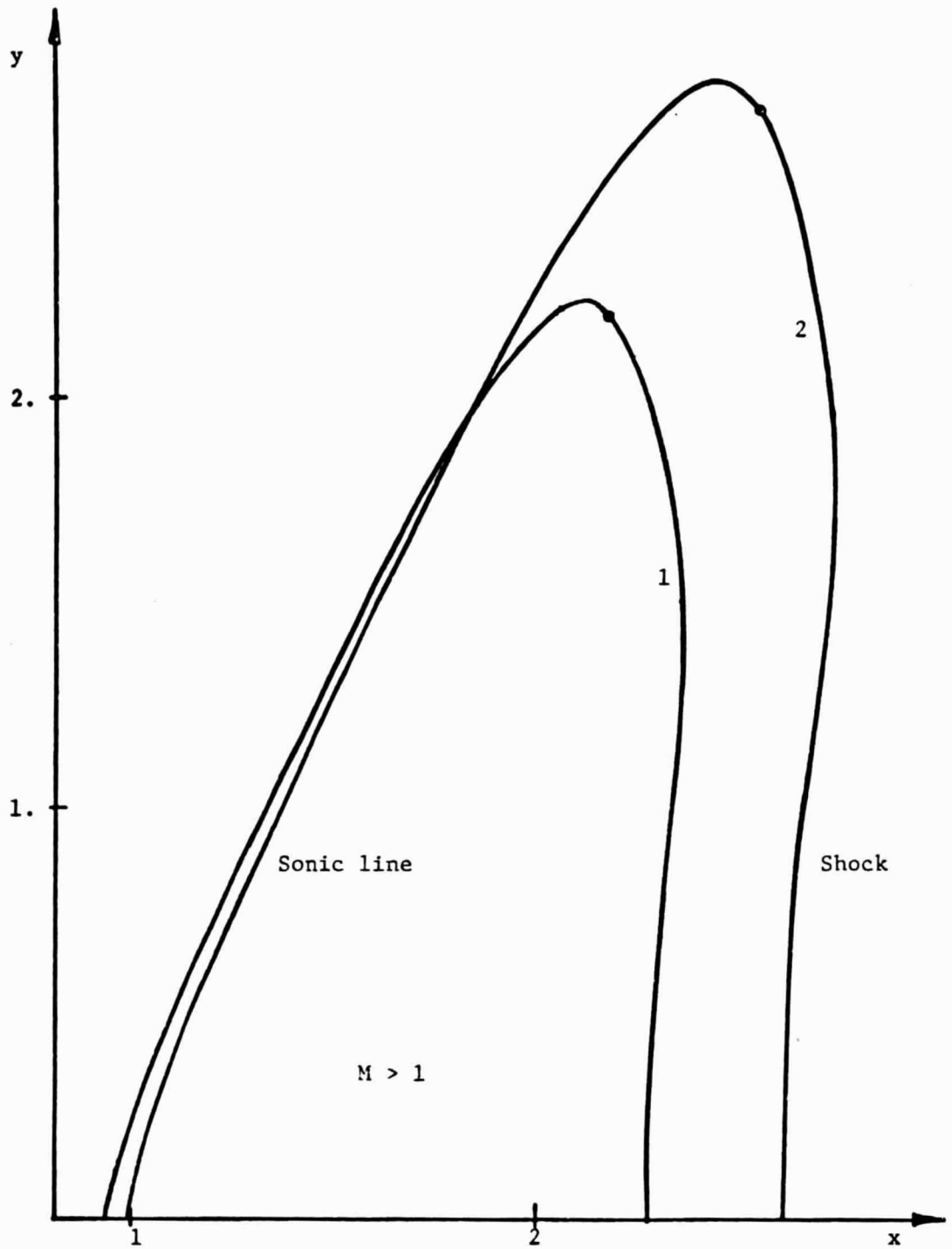

Figure 3. Sonic line and shock for flow over wedge at K = -0.5
Curve 1: non-conservative sonic point operator;
Curve 2: modified conservative scheme.

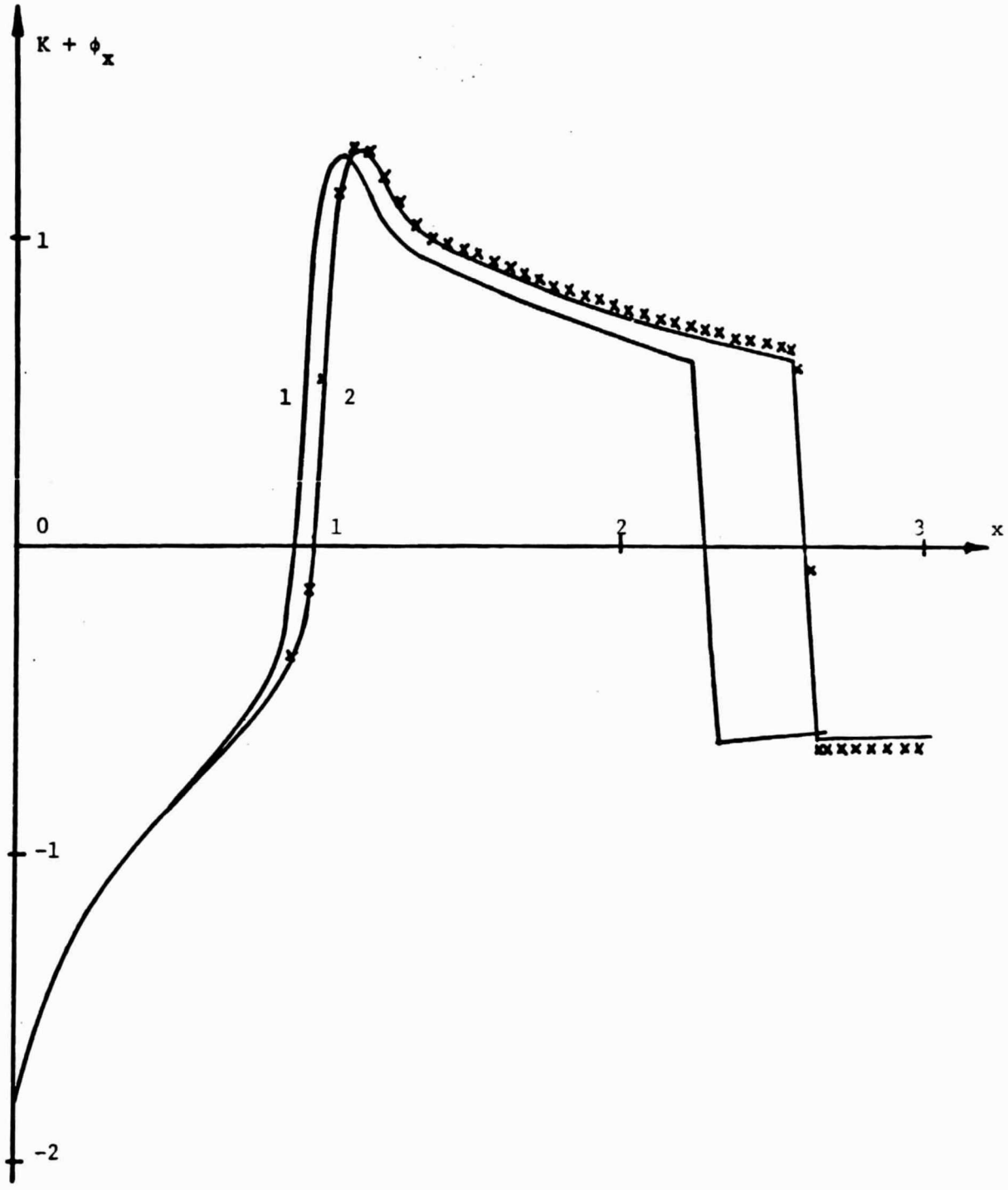

Figure 4. Pressure distribution along wedge at K = -0.5. Curve 1: non-conservative sonic point operator; Curve 2: modified conservative scheme; "x": conservative scheme with modified far-field boundary condition (note change in shock strength). See Table 2.

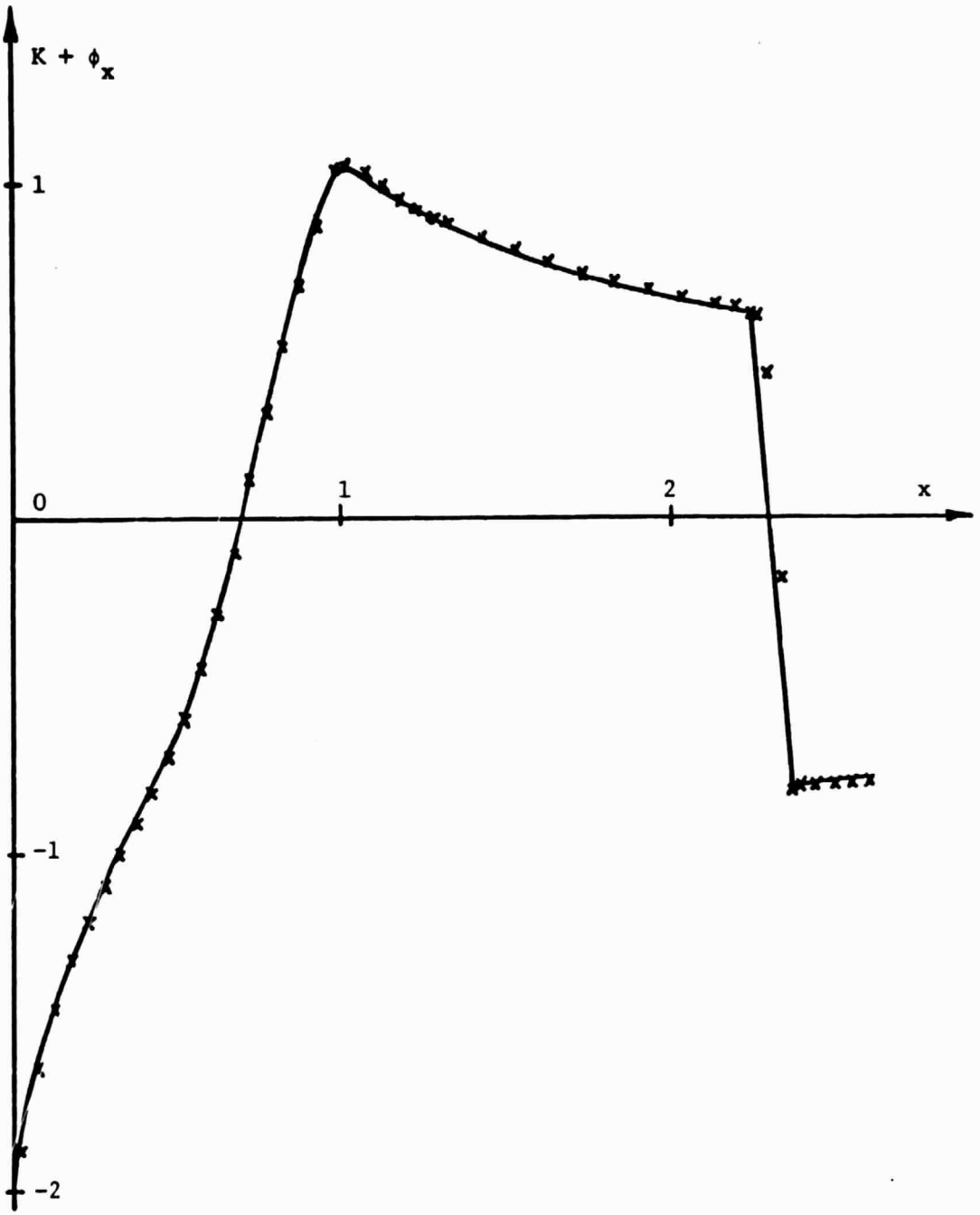

Figure 5. Pressure distribution along a smooth wedge at K = -0.5. ———: conservative scheme; "x": conservative scheme with modified far-field boundary condition.

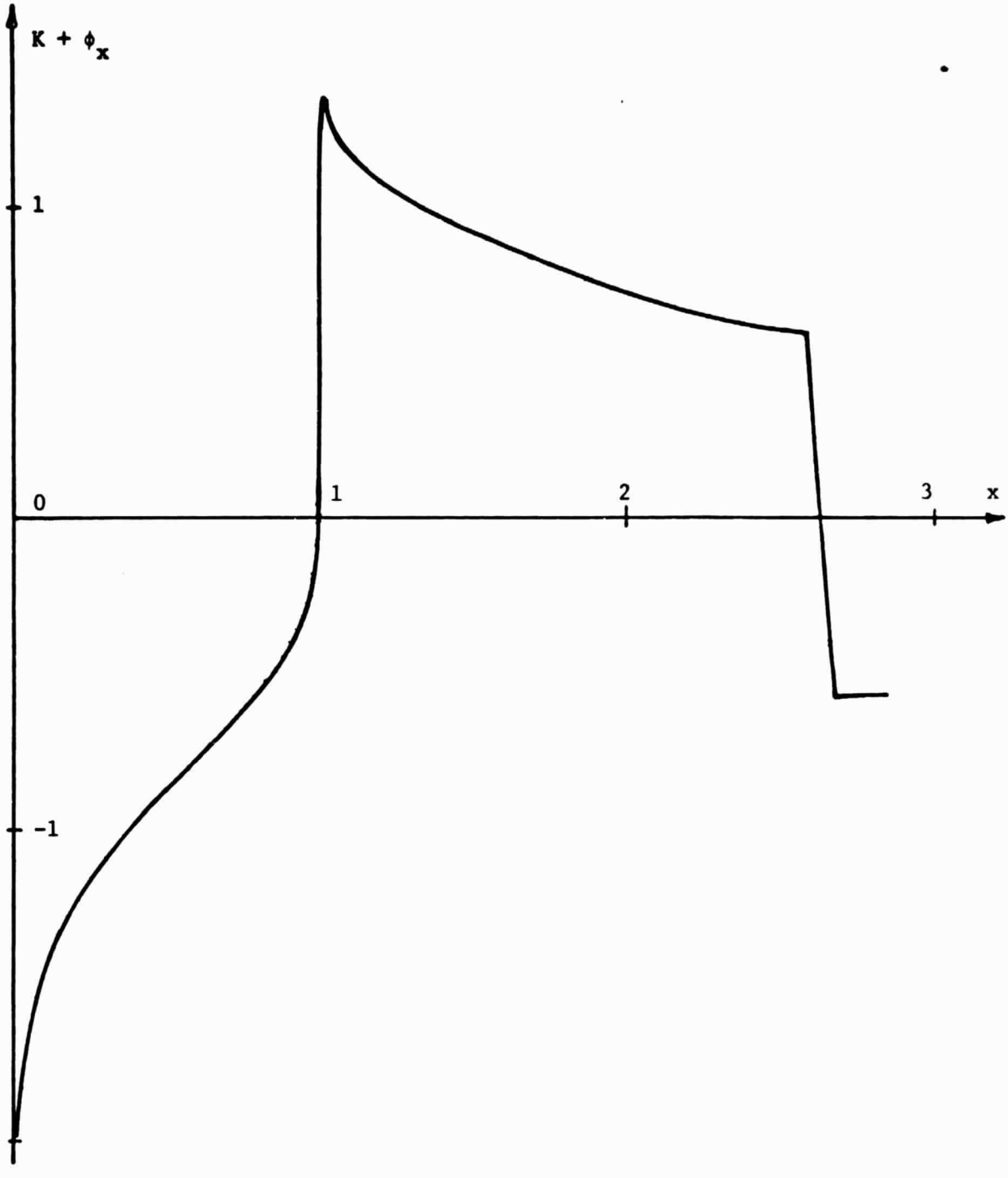

Figure 6. Pressure distribution along a wedge at K = -0.5 using non-uniform mesh calculations.

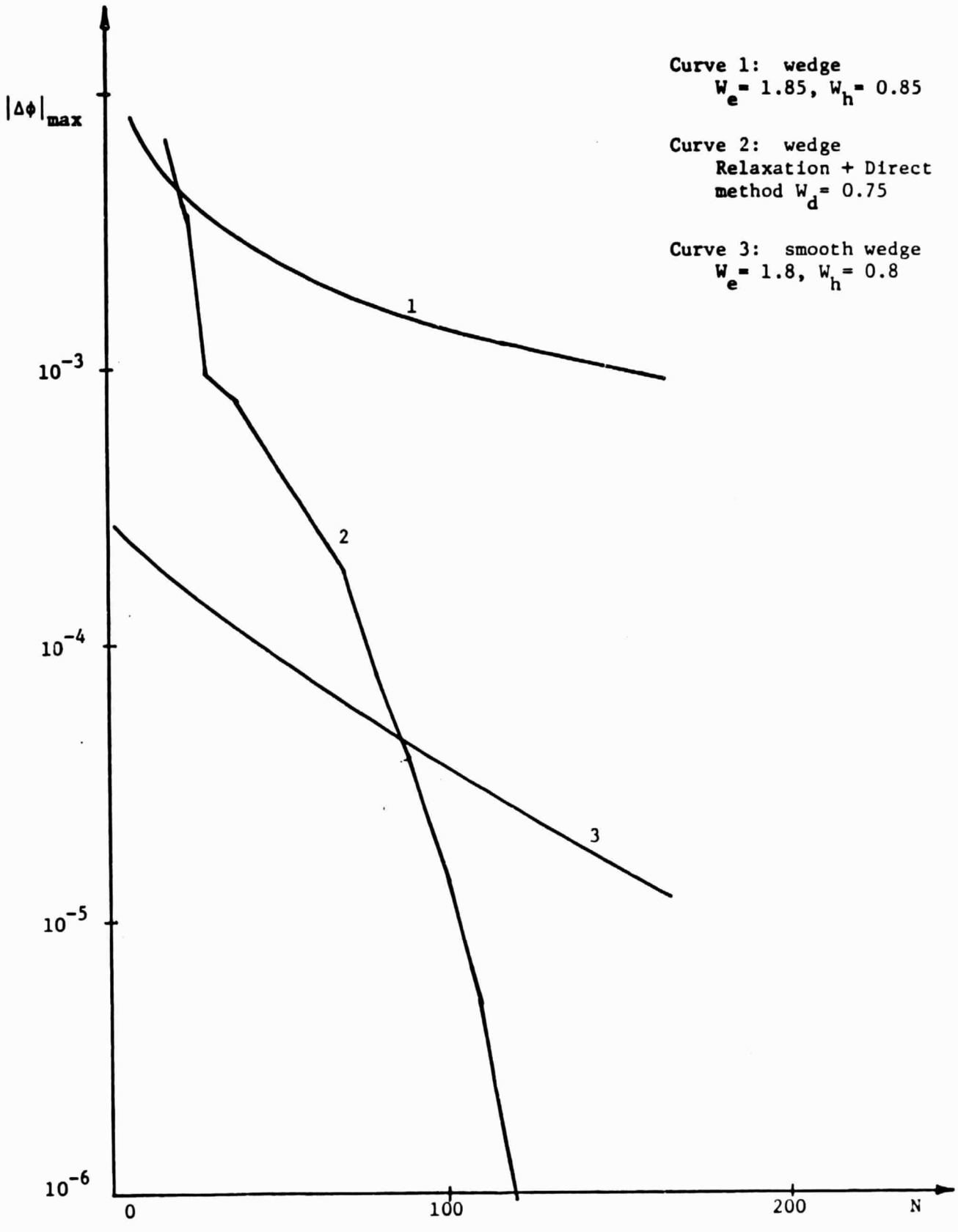

Figure 7. Error as a function of number of iterations for flow over wedge at K = -0.5.

References

1. Murman, E. M.; 1974, "Analysis of Embedded Shock Waves Calculated by Relaxation Methods," AIAA J., 12, 626-633.

2. Yu, N. J. and Seebass, A. R.; 1975, "Inviscid Transonic Flow Computations with Shock Fitting," Ed. K. Oswatitsch and D. Rues, IUTAM Symposium Transsonicum II, Göttingen.

3. Yu, N. J. and Seebass, A. R.; 1974, "Computational Procedures for Mixed Equations with Shock Waves," Ed. J. T. Oden, et al., Computational Methods in Non-linear Mechanics, Texas.

4. Hafez, M. M. and Cheng, H. K., 1975, "Convergence Acceleration and Shock Fitting for Transonic Aerodynamic Computations," AIAA paper 75-51.

5. Weatherill, W. H., Ehlers, F. E. and Sebastian, J. D.; 1975, "Computation of the Transonic Perturbation Flow Fields around Two-and Three-Dimensional Oscillating Wings," NASA, CR-2599.

6. Hockney, R. W., 1970; "The Potential Calculation and Some Applications," Methods in Computational Physics, 9, 135-211.

7. Boerstoel, J. W.; 1975, "Review of the Application of Hodograph Theory to Transonic Aerofoil Design and Theoretical and Experimental Analysis of Shock-free Aerofoils," IUTAM Symposium Transsonicum II, Göttingen.

8. Cole, J. D.; 1975, "Modern Developments in Transonic Flows," SIAM J. Appl. Math., 29, No. 4.

9. Pierpont, P. K.; 1975, "Bringing Wings of Change: NASA's Airfoil Research Program," Astronautics and Aeronautics, 10.

10. Bailey, F. R.; 1974, "On the Computation of Two- and Three-Dimensional Steady Transonic Flows by Relaxation Methods," AGARD/VKI Lecture Series on Computational Methods in Fluid Dynamics, von Karman Institute, Belgium.

11. Jameson, A.; 1975, "Numerical Computation of Transonic Flows with Shock Waves," Ed. K. Oswatitsch and D. Rues, IUTAM Symposium Transsonicum II, Göttingen.

12. Ballhaus, W. F.; 1976, "Some Recent Progress in Transonic Flow Computations," Lecture Series on Computational Fluid Dynamics, von Karman Institute, Belgium.

13. Murman, E. M. and Cole, J. D.; 1971, "Calculation of Plane Steady Transonic Flows," AIAA J. 9, No. 1, 114-121.

14. Garabedian, P. and Korn, D. G.; 1971, "Numerical Design of Transonic Airfoils," Numerical Solution of Partial Differential Equations-II, Academic Press, N. Y., 253-271.

15. Boerstoel, J. W. and Huizing, G. H.; 1974, "Transonic Shock-free Aerofoil Design by an Analytic Hodograph Method," AIAA paper 74-539.

16. Hicks, R. M., Murman, E. M. and Vanderplaats, G. N.; 1974, "An Assessment of Airfoil Design by Numerical Optimization," NASA TM X-3092.

17. Barger, R. L. and Brooks, C. W. Jr.; 1974, "A Streamline Curvature Method for Design of Supercritical and Subcritical Airfoils," NASA TN D-7770.

18. Povinelli, F. P., Klineberg, J. M. and Kramer, J. J.; 1976, "Improving Aircraft Energy Efficiency," 2, Astronautics and Aeronautics.

19. Murman, E. M. and Cole, J. D.; 1974, "Inviscid Drag at Transonic Speeds," AIAA paper, 74-540.

20. Dafermos, C. M.; 1974, "Quasilinear Hyperbolic Systems that Result from Conservation Laws," Nonlinear Waves, Ed. S. Leibovich and R. Seebass, 82-102.

21. Moretti, G.; 1975, "A Circumspect Exploration of a Difficult Feature of Multidimensional Embedded Shocks," AIAA 2nd Computational Fluid Dynamics Conference, Proceedings.

22. Klunker, E. B.; 1971, "Contribution to Methods for Calculating the Flow about Thin Lifting Wings at Transonic Speeds--Analytic Expressions for the Far Field," NASA TN D-6530.

23. Caughey, D. A. and Jameson, A.; 1976, "Accelerated Iterative Calculation of Transonic Nacelle Flowfields," McDonnell Douglas Research Lab., MDRL 76-1.

Appendix A: Construction of a Second-Order Conservative Scheme

The basic requirement for a numerical scheme to be flux conservative is that the difference equation be in divergence form. The difference approximations (15a,b) satisfy the above requirement when we substitute them into $(K + \phi_x)\phi_{xx}$, i.e.,

$$\{(K+\phi_x)\phi_{xx}\}_{i,j} = \{K + \frac{1}{2\Delta x}(2\phi_{i,j} - \phi_{i-1,j} - 2\phi_{i-2,j} + \phi_{i-3,j})\}\cdot$$

$$\{\frac{1}{\Delta x^2}(2\phi_{i,j} - 5\phi_{i-1,j} + 4\phi_{i-2,j} - \phi_{i-3,j})\}$$

$$= \frac{1}{2\Delta x}\{(K + \frac{2\phi_{i,j} - 3\phi_{i-1,j} + \phi_{i-2,j}}{\Delta x})^2 - (K + \frac{2\phi_{i-1,j} - 3\phi_{i-2,j} + \phi_{i-3,j}}{\Delta x})^2\}$$

$$= \frac{1}{2\Delta x}\{(K + \phi_x)^2_{i-1/2} - (K + \phi_x)^2_{i-3/2}\}$$

where $(K + \phi_x)_{i-1/2} = K + \frac{2\phi_{i,j} - 3\phi_{i-1,j} + \phi_{i-2,j}}{\Delta x}$.

It can easily be seen that for purely supersonic flow, the flux $(K + \phi_x)^2$ at the interface cancels exactly when the difference equations are summed with respect to i and j. This is also true for a purely subsonic region using central difference approximations, where

$$(K + \phi_x)_{i-1/2} = K + (\phi_{i,j} - \phi_{i-1,j})/\Delta x.$$

Because of the change of difference approximations at the subsonic-supersonic interface, special care has to be taken in forming the difference approximations in order to maintain the flux conservative property. Let us consider a strip of computational points, where "a"

denotes the sonic point, and "s" the shock point. For simplicity, let us assume that the supersonic region is confined in a < i < s.

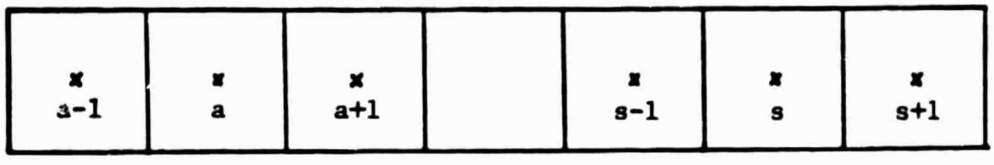

Sketch A1

The difference approximations for $(K + \phi_x)\phi_{xx}$ at each point are:

Point	Difference Approximation for $(K + \phi_x)\phi_{xx}$
a-1	$\frac{1}{2\Delta x}\left\{\left(K + \frac{\phi_a - \phi_{a-1}}{\Delta x}\right)^2 - \left(K + \frac{\phi_{a-1} - \phi_{a-2}}{\Delta x}\right)^2\right\}$
a	?
a+1	$\frac{1}{2\Delta x}\left\{\left(K + \frac{2\phi_{a+1} - 3\phi_a + \phi_{a-1}}{\Delta x}\right)^2 - \left(K + \frac{2\phi_a - 3\phi_{a-1} + \phi_{a-2}}{\Delta x}\right)^2\right\}$
. . . . .	
s-1	$\frac{1}{2\Delta x}\left\{\left(K + \frac{2\phi_{s-1} - 3\phi_{s-2} + \phi_{s-3}}{\Delta x}\right)^2 - \left(K + \frac{2\phi_{s-2} - 3\phi_{s-3} + \phi_{s-4}}{\Delta x}\right)^2\right\}$
s	?
s+1	$\frac{1}{2\Delta x}\left\{\left(K + \frac{\phi_{s+2} - \phi_{s+1}}{\Delta x}\right)^2 - \left(K + \frac{\phi_{s+1} - \phi_s}{\Delta x}\right)^2\right\}$

At point "a-1", the incoming flux $\{K + (\phi_{a-1} - \phi_{a-2})/\Delta x\}^2$ is cancelled by the outgoing flux at point a-2, the flux that remains uncancelled is $\{K + (\phi_a - \phi_{a-1})/\Delta x\}^2$, which has to be cancelled by the difference approximations at "a". Similarly, the uncancelled flux at point "a+1" is

$$- \left(K + \frac{2\phi_a - 3\phi_{a-1} + \phi_{a-2}}{\Delta x}\right)^2 .$$

Therefore, the only choice of difference approximations for $(K+\phi_x)\phi_{xx}$ at point "a" that conserves mass is

$$\{(K+\phi_x)\phi_{xx}\}_a = \frac{1}{2\Delta x}\left\{\left(K + \frac{2\phi_a - 3\phi_{a-1} + \phi_{a-2}}{\Delta x}\right)^2 - \left(K + \frac{\phi_a - \phi_{a-1}}{\Delta x}\right)^2\right\}$$

$$= \left\{K + \frac{3\phi_a - 4\phi_{a-1} + \phi_{a-2}}{2\Delta x}\right\}\left\{\frac{\phi_a - 2\phi_{a-1} + \phi_{a-2}}{\Delta x^2}\right\},$$

which is given by (16a,b).

Similarly, at shock point "s",

$$\{(K+\phi_x)\phi_{xx}\}_s = \frac{1}{2\Delta x}\left\{\left(K + \frac{\phi_{s+1} - \phi_s}{\Delta x}\right)^2 - \left(K + \frac{2\phi_{s-1} - 3\phi_{s-2} + \phi_{s-3}}{\Delta x}\right)^2\right\}$$

$$= \left\{K + \frac{\phi_{s+1} - \phi_s + 2\phi_{s-1} - 3\phi_{s-2} + \phi_{s-3}}{2\Delta x}\right\}\left\{\frac{\phi_{s+1} - \phi_s - 2\phi_{s-1} + 3\phi_{s-2} - \phi_{s-3}}{\Delta x^2}\right\} .$$

To insure the correct transition, the type dependent coefficient $K + \phi_x$ is tested at each computational point by

$$q_c = (K + \phi_x)_c = K + (\phi_{i+1} - \phi_{i-1})/2\Delta x$$

$$q_b = (K + \phi_x)_b = K + (\phi_i - \phi_{i-2})/2\Delta x,$$

where the sonic point is defined by $q_c > 0$, and $q_b < 0$, and the shock point by $q_c < 0$, $q_b > 0$.

Appendix B: Shock Fitting

A shock fitting scheme can easily be implemented in the relaxation calculations. We introduce shock fitting when a reasonably well-converged first-order result is obtained. The initial shock position is determined by interpolating the sonic position in the supersonic to subsonic transitions, and the shock points are then treated as regular computational points. (Sketch B1). At the shock point, the flow properties ahead of the shock, i.e., ϕ_x, ϕ_y can be determined either by extrapolation from the upstream conditions at Q and R, or by using the characteristic relations along c^+ and c^-. Both methods have been tested and have given satisfactory results. For most of the calculations, the simple extrapolation method was used. Behind the shock, $\hat{\phi}_y$ is extrapolated by the usual difference method using the old value at P, and $\hat{\phi}_x$ is obtained from the jump relation (3). Should the shock slope extrapolation provide a shock intersection at s' as indicated by the dotted line, then the value of ϕ is fixed at s' by using the value of ϕ, $\hat{\phi}_x$, $\hat{\phi}_y$ at s. At each stage of the calculation we correct the position of the shock by the simple procedure

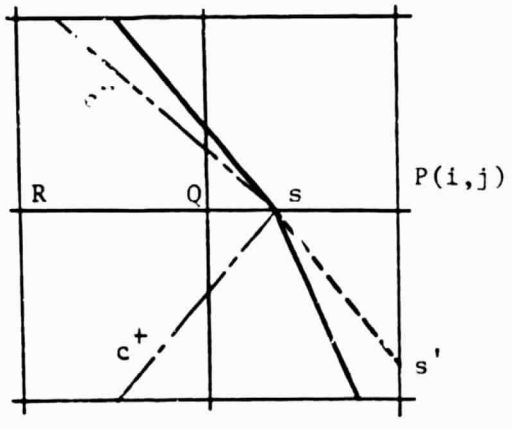

Sketch B1

$$x_s^{n+1} = x_s^n + k\Delta x\ (\phi_x^{n+1} - \phi_x^n)_s. \qquad \text{(B-1)}$$

Various values of k have been tried; values near one seem to be the most satisfactory. The rationale for (B-1) is simple: if the flow

ahead of the shock has increased in speed, i.e., $\phi_x^{n+1} - \phi_x^n > 0$, (B-1) allows the shock to be swept downstream and flow properties can be recalculated using the new shock position.

Because the shock is treated as a discontinuity, the flow ahead of and behind the shock is continuous. Thus, the difference approximations for the grid points adjacent to the shock point, e.g., P and Q can be constructed using the usual difference approximations without taking into consideration the exact internal flux cancellation. Numerical tests showed that if the difference approximations at P and Q are consistent with the differential equation, the internal fluxes generated at those points are small.